NORCE Norwegian Research Centre AS
www.norceresearch.no

# Assessment of calibrated Sentinel-1 OCN RVL products

**Author:** H. Johnsen

**Rapport:** 1-2022 Energy and Technology

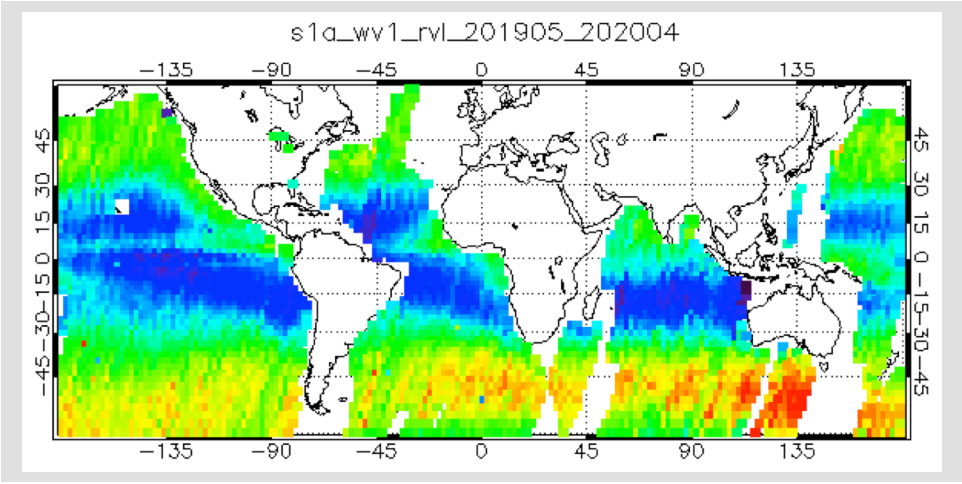


Project Team: H. Johnsen[1], G. Engen[1], G. Guitton[2], F. Collard[3], A.Recchia[3], A. Cotrufo[3]

S. Bras[4], N. Miranda[5], M. Pinheiro[5]

[1]NORCE Norwegian Research Center AS, Tromsø, Norway.

[2]OceanDataLab Ltd., Locmaria Plouzane, France.

[3]Aresys Ltd, Milano, Italy

[4]ESTEC/ESA, Noordwijk, The Netherlands

[5]ESRIN/ESA, Frascati, Italy

This work is performed under ESA-ESRIN contract No. 4000123040/18/I-BG-SENTINEL-1 RVL. We would like to thank EU Copernicus program for providing open access to the Sentinel-1 products.

| | |
|---|---|
| Report title | Assessment of calibrated Sentine-1 OCN RVL products |
| Project No | 101854 |
| Institution | NORCE Energy & technology – Earth Observation |
| Client(s) | European Space Agency - ESRIN |
| Classification: | Open |
| Report No. | 1-2022 |
| ISBN | 978-82-8408-194-6 |
| No. of pages | 22 |
| Keywords | Sentinel-1, Doppler frequency, Radial Velocity |

Summary

The accuracy and precision of the calibrated DC frequency of S1 WV and IW acquisitions are assessed using data acquired over both land and ocean areas. Data from the period of 1st of May 2019 until 30th of April 2020 are used. For WV mode the assessment is performed on global data, while for IW mode the assessment is performed for data acquired over supersites (Skagerak (Norway) and Agulhas (South-Africa)). The DC standard deviation (STD) and bias show significant reduction for both satellites and for all swaths. Assessment of the performance of global WV data shows a STD (precision) around 6Hz, while the BIAS (accuracy) is less than 2 Hz. The performance is very similar for both satellites and for both swaths. For IW the STD is similar, but the bias is slightly higher and small DC biases between sub-swaths are sometimes observed.
Front page: Mean radial velocity derived from S1a WV1 data.

## Revisions

| Rev./ Rev. | Dato/ Date | Forfatter/ Author | Kontrollert av/ Checked by | Godkjent av/ Approved by | Årsak til revisjon/ Reason for rev. |
|---|---|---|---|---|---|
| 1.0 | 31.01.2021 | H. Johnsen | Heidi Hindberg | Kjell Arild Høgda | |

# Content

**1. INTRODUCTION ..... 4**

**2. DATA AND METHODOLOGY ..... 5**

2.1. S-1 Doppler Centroid Frequency Calibration ..... 5

**3. RESULTS ..... 8**

3.1. S1 WV Mode ..... 8

3.2. S1 IW Mode ..... 13

**4. SUMMARY ..... 21**

## Abstract

The Doppler Centroid (DC) frequency shift recorded over ocean surfaces by Synthetic Aperture Radar (SAR) is a sum of contributions from satellite attitude/antenna and ocean surface motion induced by waves and underlying ocean currents. A precise calibration of the DC is needed in order to predict and subsequently remove contributions from attitude/antenna.

Recently, a novel data calibration technique based on combining gyroscope telemetry data and global Sentinel-1 WV OCN products (OceanDataLab Ltd, 2019), has demonstrated promising capabilities to quantify the Sentinel-1 (S1) attitude and hence provide calibrated estimates of the corresponding DC frequency shift. One year of S1 a and b WV OCN products, orbit data and gyroscope data are combined providing one year of estimated attitude data (AUX_ESTATT). For the same time period, mean DC bias versus elevation angle is computed on a daily basis from S1 IW land acquisitions (AUX_DCBIAS).

The AUX_ESTATT and AUX_DCBIAS products are subsequently used to generate global data set of calibrated S1 WV OCN products as well as sub-sets of calibrate S1 IW OCN products from predefined super sites (Norwegian Coast, Agulhas, Mediterranean). In this paper we assess the accuracy and precision of the calibrated DC frequency of S1 WV and IW acquisitions acquired over both land and ocean areas. The DC standard deviation (STD) and bias show significant reduction for both satellites and for all swaths. Assessment of the performance of global WV data shows a STD (precision) around 6Hz, while the BIAS (accuracy) is less than 2 Hz. The performance is very similar for both satellites and for both swaths. For IW the STD is similar, but the bias is slightly higher and small DC biases between sub-swaths are sometimes observed.

The remaining challenge is mainly due to change in antenna characteristics on a timescale not captured with the procedure used to generate the mean DC bias stored in the AUX_DCBIAS file. Such changes may come from the thermo-elastic effects and/or temperature compensations applied to the antenna. This directly affects the IW mode DC, where it is also clearly visible in some scenes. For WV mode it mainly impacts the statistics.

We conclude that S1 WV mode has achieved a performance (i.e. accuracy and precision) within the requirement for climatology mapping of global ocean current features. For IW mode, we have achieved a precision within the requirement, but use of land areas within the scene is still required to achieve the required accuracy over all sub-swaths.

# 1. Introduction

Synoptic maps of ocean surface wind, waves and current from space are important inputs to better characterization and parameterizations of oceanic mesoscale and sub-mesoscale dynamics as well as support to advances in ocean-atmosphere research and modelling activities (Bourassa et. al., 2019). In coastal ocean areas the current is usually measured from in situ surface drifters (Lagrangian), fixed moorings (ADCP) (Eulerian), and land-based HF-radars (Eulerian) (Ardhuin F. et. al., 2009), (Röhrs J. et. al., 2015). However, these measurements are irregular in time and space and cover only a limited area yielding observation gaps. Several spaceborne SAR missions such as TerraSAR-X (Romeiser R. et. al., 2010), Tandem-X (Romeiser R. et. al., 2014), Envisat (Chapron et. al., 2005), (Johannessen J. et. al., 2008) have shown the capability to provide measurements of the radial component of mean Lagrangian surface velocity vector. The encouraging results of these previous missions led to the development of a specific Doppler product for the S1 missions (i.e. S1 OCN RVL product) (Engen and Johnsen, 2015), (Sentinel-1 Product Specification, 2020).

Sentinel-1 is an operational constellation of two SAR missions (A and B) providing continuous all-weather, day-and-night imagery at C-band with improved revisit time, geographical coverage and rapid data dissemination to support operational marine monitoring and applications. Unfortunately, it was not possible to achieve a calibrated S1 OCN RVL product based on the strategy implemented into the S1 Level 2 IPF processor (Johnsen et. al. 2016), (Moiseev et. al. 2019). This because the attitude DC computed from the downlinked quaternions and the DC bias from the antenna model were not precise and accurate enough. This deficit initiated the development of a novel Sentinel-1 DC calibration strategy based on combining the DC observations with the gyroscope telemetry data. The methodology has demonstrated capabilities to quantify the satellite attitude and hence provide reliable estimates of the Doppler shift (OceanDataLab, 2018), (Moiseev et. al. 2020). Recently, the calibration methodology has been made semi-operational allowing production of massive calibrated S1 OCN RVL datasets.

In this study, we take advantage of the calibrated S1 WV OCN RVL dataset, the data driven antenna DC bias product, and the estimated attitude data product. From this data set we can recalibrate and assess the performance of any of the S1 OCN RVL products acquired within the same time period. Section 2 describes the data set used and the calibration methodology of the Sentinel-1 DC observations. Section 3 presents the assessment results based on both ocean and land data. Discussion and conclusions are presented in Section 4.

# 2. Data and Methodology

The estimated S1 a,b attitude data product used in this study is generated for the period of 01 May 2019 to 30 April 2020. The WV products are obtained along two swaths centred at incidence angles of $\theta = 23°$ (from 21.6° to 25.1°, WV1) and $\theta = 36°$ (from 34.8° - 38.0°, WV2). The acquisitions are repeated every 100 km (within a swath), each covering an area of 20x20 km$^2$. The WV OCN RVL product used here has a resolution of 20x20 km$^2$. The IW products cover three sub-swaths with incidence angles between 30 to 42 degrees and a swath width of 250 km. The OCN RVL product used here has a pixel resolution of 1.5x1.5km$^2$. The estimated attitude information is provided in AUX_ESTATT netCDF files, and the DC bias is provided in the AUX_DCBIAS netCDF files. The AUX_DCBIAS product is computed regularly over land areas (daily) from the L1 IPF DC estimates annotated in the S1 L1A products. The DC bias characterizes those effects that cannot be measured from the gyro rates, such as seasonally DC trends and contribution introduced by antenna electronic miss-pointing. All data used in this study is described in Table 1.

**Table 1.** *Datasets Used in the Study. All data is provided by ESA/Copernicus*

| Dataset | Source | Time Resolution | Spatial Resolution | Parameter | Area |
|---|---|---|---|---|---|
| S1 DC frequency | S1a, b WV OCN product | 6 days | 20 km | Doppler shift [Hz], | Global |
| S1 DC frequency | S1a, b IW OCN product | < 6 days | 1.5 km | Doppler shift [Hz] | Regional |
| S1 a, b attitude variation | AUX_ESTATT | 2 sec. | - | Roll, pitch and yaw deviation angles [deg.] versus elevation angle. | Global |
| S1 a, b antenna DC biases | AUX_DCBIAS | Daily | - | DC [Hz] versus off-boresight angle | Global |

## 2.1. S-1 Doppler Centroid Frequency Calibration

The Sentinel-1 estimated DC ($f_{dc}$) could be partitioned into contributions from antenna, orbit/attitude and geophysics. The DC partitioning can be expressed by the following terms:

$$f_{dc} = f_{bias}(\beta) + f_{att}\left(\beta, \theta_{att}(t)\right) + \Delta f_{bias}(T) + \underbrace{(f_{osc} + f_{ss})}_{f_{rvl}} \quad (1)$$

Here

- $f_{att}$ is the fast time varying part of the Doppler signal (period << orbital period) dependent on the satellite attitude deviation from nominal steering. This parameter is computed as described in eq.(2). Here $\theta_{att}(t)$ is the AOCS attitude roll, pitch and yaw errors at time t. This term also includes residual variations along orbit estimated by fitting one harmonic at orbital period plus a constant DC bias per orbit. The constant bias is given in the auxiliary attitude file (AUX_ESTATT).
- $f_{bias}$ is the low-frequency (period >> orbital period) Doppler signal (bias) related to antenna electronic miss-pointing and low frequency attitude variation. This parameter is generated daily from data acquired over homogenous land areas (rain forest) and provided by the DC bias auxiliary product (AUX_DCBIAS).
- $\Delta f_{bias}$ is a change in DC frequency caused by temperature (T) compensation applied to antenna during acquisition. It is so far no proven means to predict this effect.
- $f_{rvl}$ is geophysical signal related to the ocean surface radial velocity (RVL) due to the combined wave-induced motion bias ($f_{ss}$) and the underlying mean Lagrangian ocean surface current ($f_{osc}$).
- $v$ is the S-1 velocity
- $f_c$ is the S1 radar frequency
- $c$ is the speed of light
- β is off-boresight angle, computed from the satellite orbit geometry.

The fast attitude term of eq.(1) can be written as:

$$f_{att} = \frac{2vf_c}{c}\left(-\Delta\theta_y(t)\cdot sin\,\beta + \Delta\theta_p(t)\cdot cos\,\beta\right) \quad (2)$$

Here

- $\Delta\theta_p(t)$ is the pitch deviation (from reference steering angle computed using EOCFI) angles derived from the gyroscope telemetry data. $\Delta\theta_p$(t) is provided by the auxiliary attitude file.
- $\Delta\theta_y(t)$ is the yaw deviation (from reference steering angle computed using EOCFI) angles derived from the gyroscope telemetry data. $\Delta\theta_y(t)$ is provided by the auxiliary attitude file.

The flowchart of the calibration procedure starting from the OCN product is shown in Figure 1. Details on how the AUX_ESTATT and AUX_DCBIAS are generated can be found in (OceanDataLab Ltd, 2019).

Over land area the last term on the right-hand side of eq.(1) is zero, and we can simply evaluate the accuracy and precision of the calibration process by analysing data acquired over land areas. Fortunately, we have also large number of S1 WV acquisitions over land areas, in particular for S1a.

Over ocean areas we can predict and removed the geophysical contribution in eq.(1) using a geophysical forward model function (CDOP) [Moiseev et. al., 2020], and evaluate the residual DC. A consistency between the land and ocean data should be achieved.

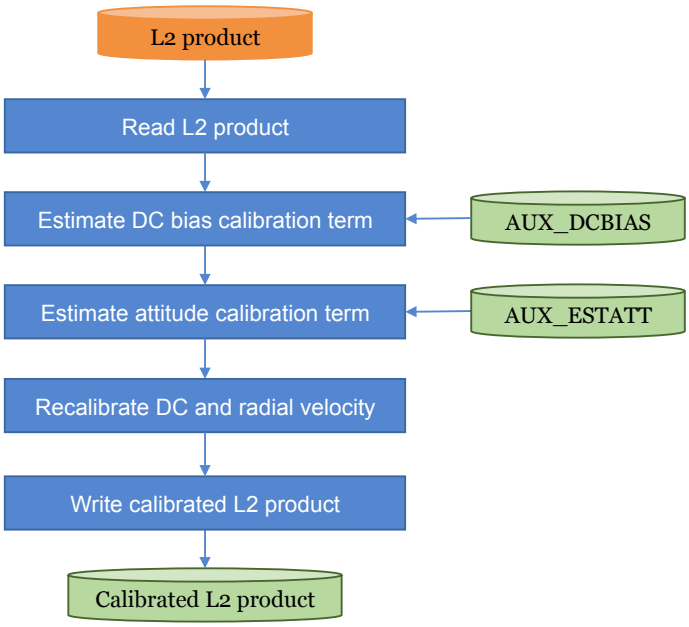


Figure 1: Flowchart of calibration of S1 OCN product using estimated attitude and DC bias auxiliary files.

# 3. Results

## 3.1. S1 WV Mode

### Land Acquisitions:

The performance analysis presented for WV mode is based on one year of S1 a, b WV data acquired globally including also land areas. For S1a land acquisitions were acquired over Australia, North-America, Amazonas, Africa, while for S1b land acquisitions where mostly acquired over Australia. Figure 2 shows the acquisitions areas and the mean calibrated DC within this period.

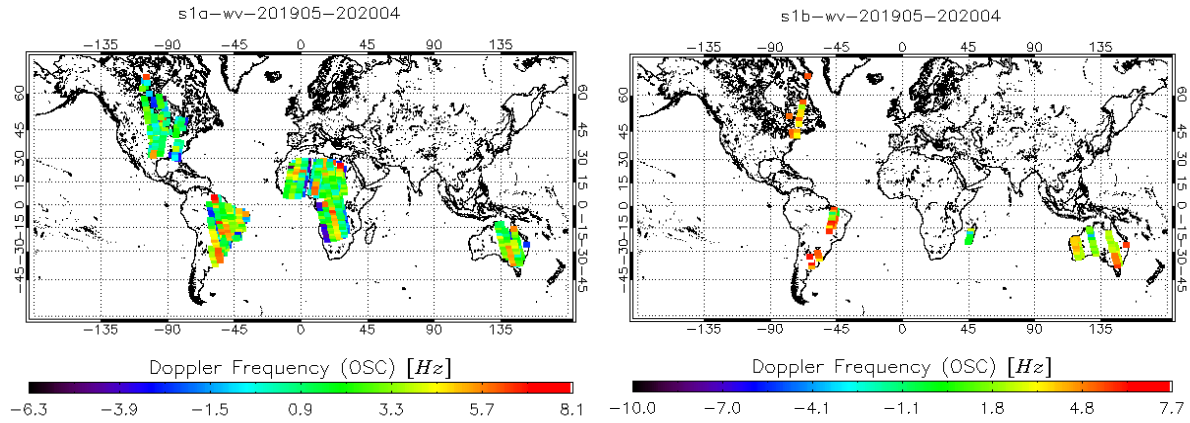


Figure 2: Mean calibrated DC acquired over land areas within the period 01.05.2019 to 30.04.2020 from S1a WV (left) and S1b WV (right).

The histograms of S1 WV OCN RVL DC before and after calibration are shown in Figure 3 for global land acquisitions of Figure 2. Figure 4 shows the same, but only over Australia. Note that there are significant more WV acquisitions over land by S1a than by S1b, but over Australia the number of acquisitions is similar.

Figures 3 and 4 show that the standard deviation and bias are significantly reduced for both satellites and for both swaths. The standard deviation is now around or less than 6Hz, and the bias only a few Hz. The results are summarized in Table 2.

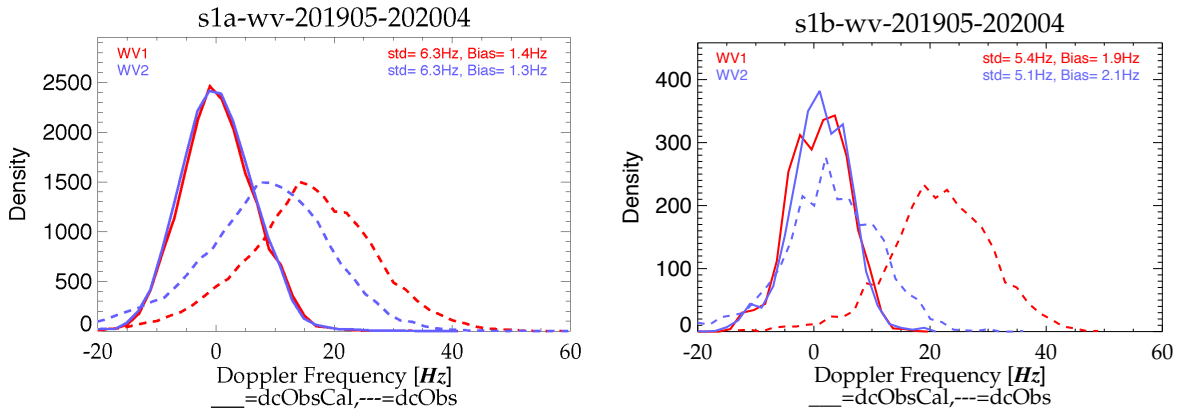


a) b)

Figure 3: Histograms of S1a (left) and S1b (right) WV OCN RVL DC frequency before and after calibration. The data was acquired between 1st May 2019 and 30th April 2020 over global land areas.

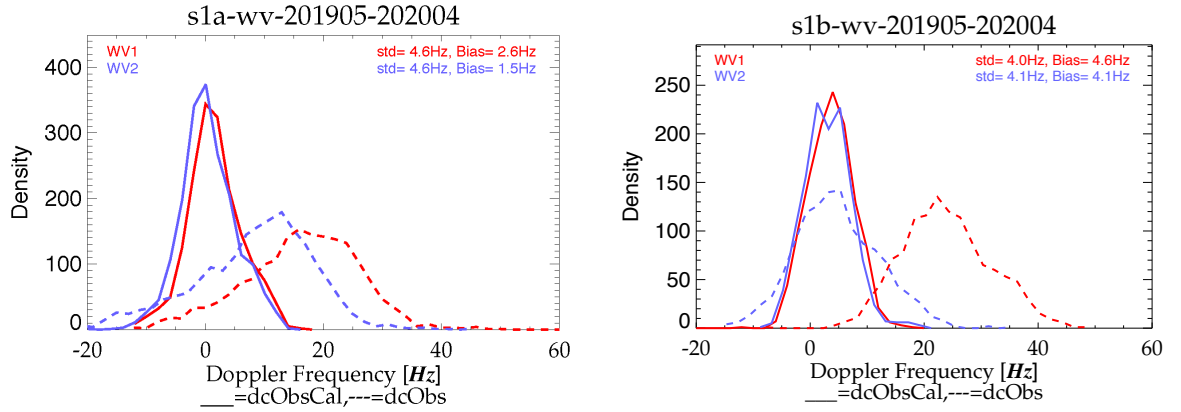


a) b)

Figure 4: Histograms of S1a (left) and S1b (right) WV OCN RVL DC frequency before and after calibration. The data was acquired between 1st May 2019 and 30th April 2020 over Australia.

Table 2: Overall performance of S1a, b WV calibrated OCN RVL product

| S1a WV -Global | | | | | | | |
|---|---|---|---|---|---|---|---|
| WV1 | | | | WV2 | | | |
| STD [Hz] | | Bias [Hz] | | STD [Hz] | | Bias [Hz] | |
| Before | After | Before | After | Before | After | Before | After |
| 11.0 | 6.3 | 16.8 | 1.4 | 11.2 | 6.3 | 9.1 | 1.3 |

| S1b WV -Global | | | | | | | |
|---|---|---|---|---|---|---|---|
| WV1 | | | | WV2 | | | |
| STD [Hz] | | Bias [Hz] | | STD [Hz] | | Bias [Hz] | |
| Before | After | Before | After | Before | After | Before | After |
| 8.8 | 5.4 | 22.7 | 1.9 | 8.5 | 5.1 | 3.9 | 2.1 |

| S1a WV -Australia | | | | | | | |
|---|---|---|---|---|---|---|---|
| WV1 | | | | WV2 | | | |
| STD [Hz] | | Bias [Hz] | | STD [Hz] | | Bias [Hz] | |
| Before | After | Before | After | Before | After | Before | After |
| 9.6 | 4.6 | 17.4 | 2.6 | 10.1 | 4.6 | 9.2 | 1.5 |

| S1b WV - Australia | | | | | | | |
|---|---|---|---|---|---|---|---|
| WV1 | | | | WV2 | | | |
| STD [Hz] | | Bias [Hz] | | STD [Hz] | | Bias [Hz] | |
| Before | After | Before | After | Before | After | Before | After |
| 7.8 | 4.0 | 24.9 | 4.6 | 7.4 | 4.1 | 5.8 | 4.1 |

Examples of attitude DC and the impact of the attitude correction on single orbit segments are exemplified in Fig.5. We note that the attitude variation along the orbit segments is more than 20 Hz in these cases.

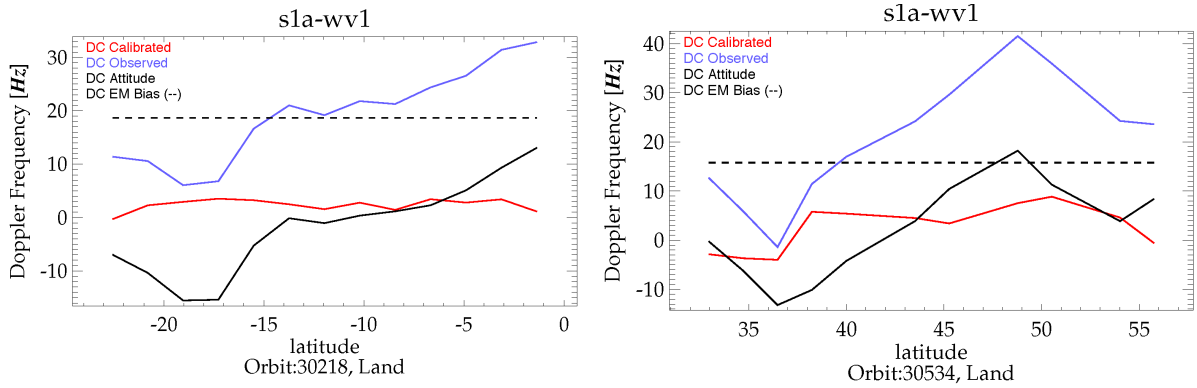


a) b)

Figure 5: Examples of S1a (a) and S1b (b) WV mean DCs along orbit segment acquired over land areas.

It is also of interest to see where the remaining variations of DC come from. In Fig. 6 we show examples of the mean calibrated DC pr. orbit segment over land, where the vertical bars show the standard deviation over the orbit segment. We observe that the mean standard deviation over the orbit segment is less than 3 Hz, while the overall standard deviation is up to 5.8 Hz. This indicates that the methodology used to capture the sub-orbital trends does not capture all the variations. Such variations may come from residual attitude contribution plus thermo-elastic effects on the antenna as well as temperature compensation applied to the antenna. Some residual attitude contribution may arise because of not optimal use of the gyros and/or a not optimal refinement with WV observations.

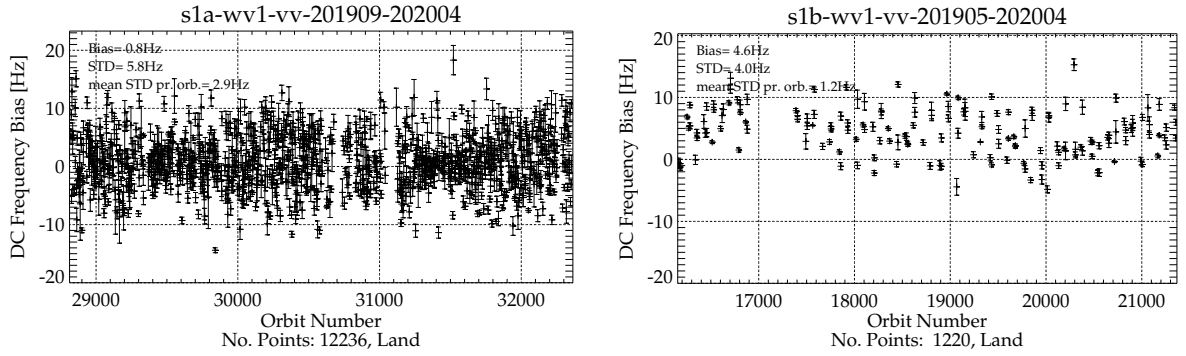


a) b)

Figure 6: Examples of S1a (a) and S1b (b) WV mean calibrated DC pr. orbit. The vertical bars indicate the standard deviation over the orbit segment.

## Ocean Acquisitions:

The calibrated S1 WV data sets contain also an estimate of the wave-induced motion bias ($f_{ss}$) (see eq.(1)). This function was derived empirical from the data set, and subsequently used to remove the geophysical DC variation along the orbits. The function allows us to compute the DC frequency of the radial ocean surface current component, $f_{osc}$ from the DC of the radial velocity, $f_{rvl}$. In Fig.7 we show S1b mean DC of the radial velocity and the mean DC of the radial ocean surface current within the period 01.05.2019 to 30.04.2020 for ascending and descending passes. From the right plots of Fig.7 we see the signature of the equatorial current.

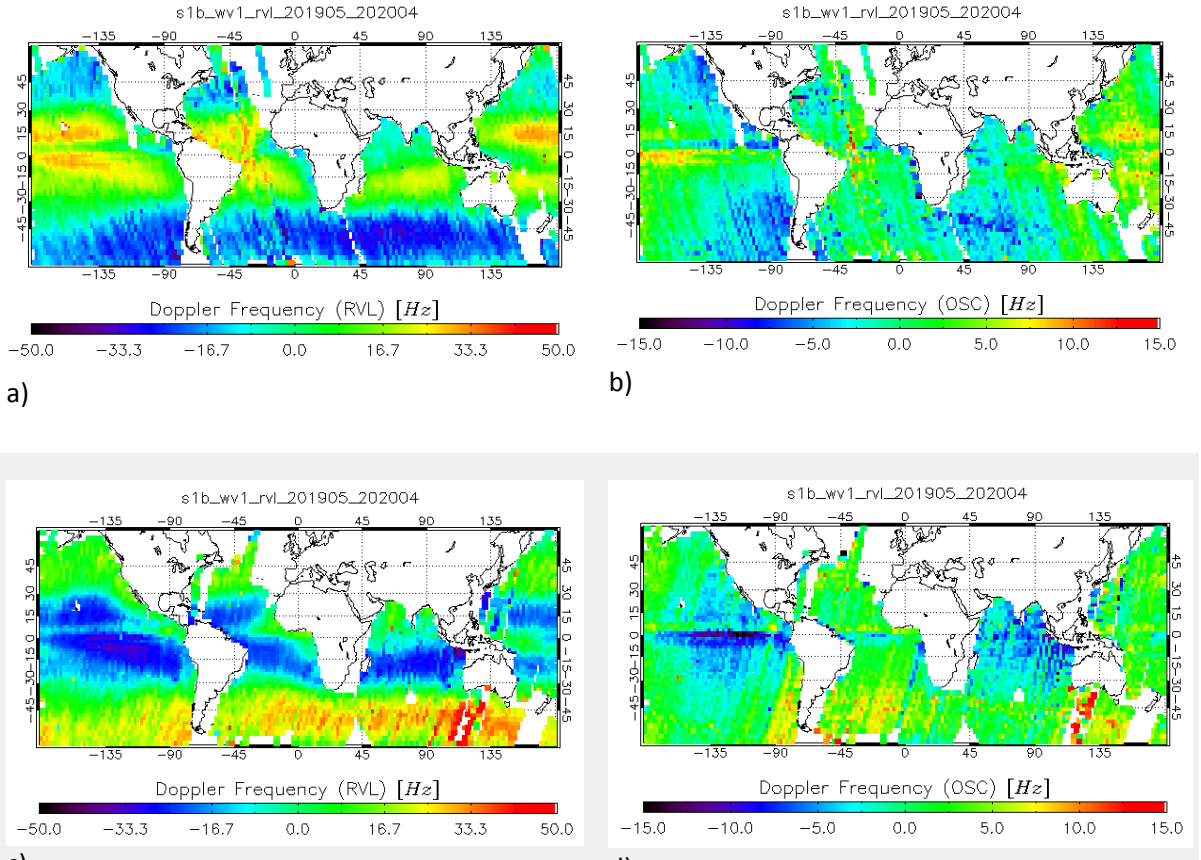


Figure 7. Mean DC of the radial velocity (a),(c) and the mean DC of the radial surface current (b),(d) derived from S1b WV1 between 01.05.2019 and 30.04.2020 in ascending (upper) and descending (lower) passes.

## 3.2. S1 IW Mode

### Land Acquisitions:

For the IW mode a large number of acquisitions over coastal areas as well as pure land areas are calibrated and validated. In particular we processed a few S1a IW and S1b IW long data takes over southern part of Africa to better evaluate the estimated attitude DC and its impact on the DC calibration along track. Examples of the Doppler frequency before and after calibration as well as the estimated attitude DC are shown in Figures 7 and 8. We observed that the attitude DC shows a variation of more than 10Hz within these orbit segments, and that the attitude DC captures well the along track trends observed in DC frequency of the OCN RVL product. The calibrated DC shows a relative constant behaviour except in areas where the observed DC shows sudden jump caused by antenna temperature compensation. This latter effect is the main remaining obstacle for achieving a well calibrated S1 IW OCN RVL product. These jumps in DC indicate that there is a change in antenna characteristics that are on a timescale not capture with the procedure used to generate the mean DC bias stored in the DC auxiliary product.

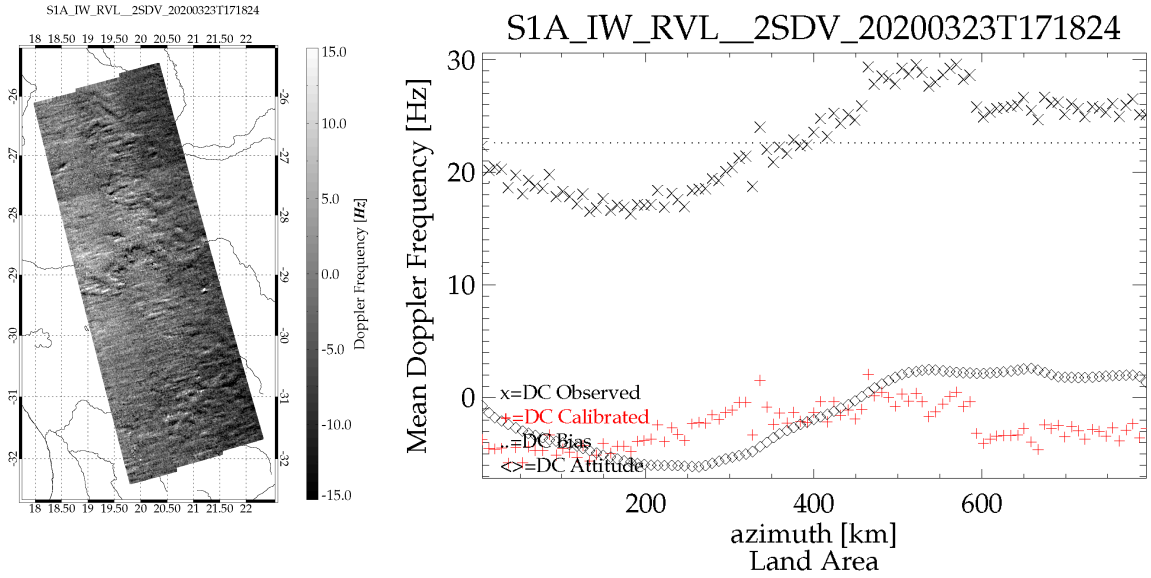

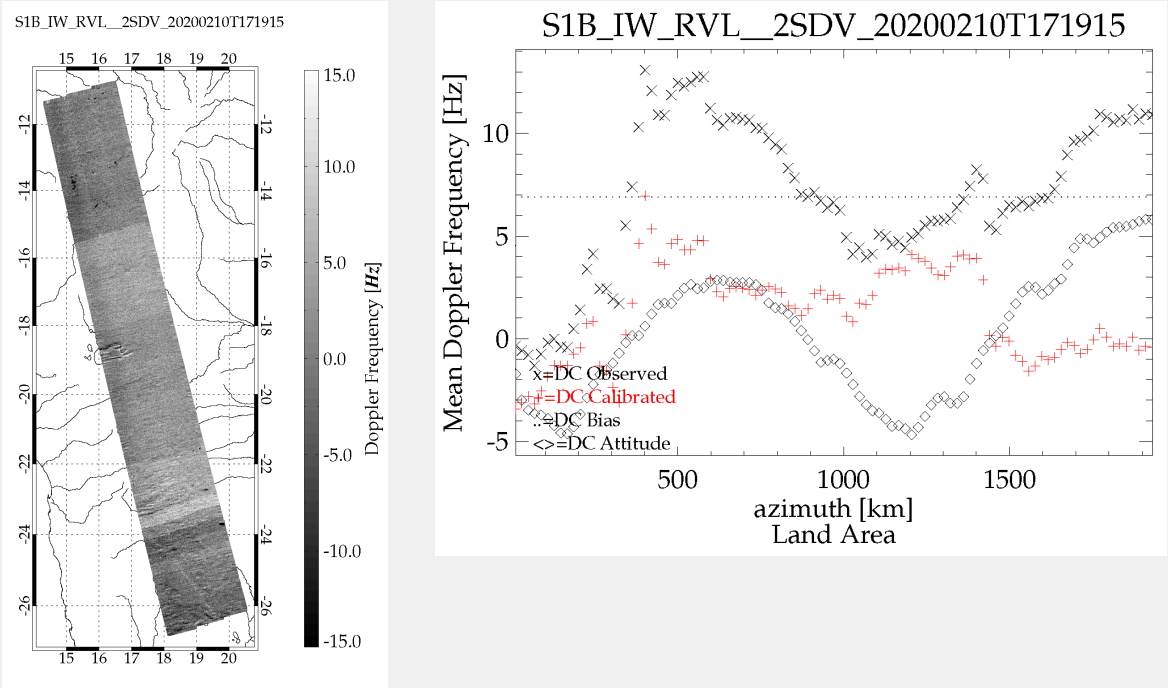


Figure 7: Left: S1 IW calibrated DC image. Right: S1 IW mean DC profiles along track. S1a upper figure, and S1b lower figure.

## Coastal Acquisitions:

For the IW mode a large number of acquisitions over coastal areas (Norwegian Coast, South-African Coast) are calibrated and validated. We evaluate mean DC over the swaths and along track before and after calibration. In Figure 8 to 11 we show examples of calibrated DC from S1a and S1b IW modes acquired over Skagerak and Agulhas. We also show the corresponding mean DC range profiles (across and along track) before and after calibration. The overall performance of the calibrated S1 IW OCN RVL products is presented Table 3 and Table 4. The data used in Table 3 and Table 4 are all acquired over pure land areas.

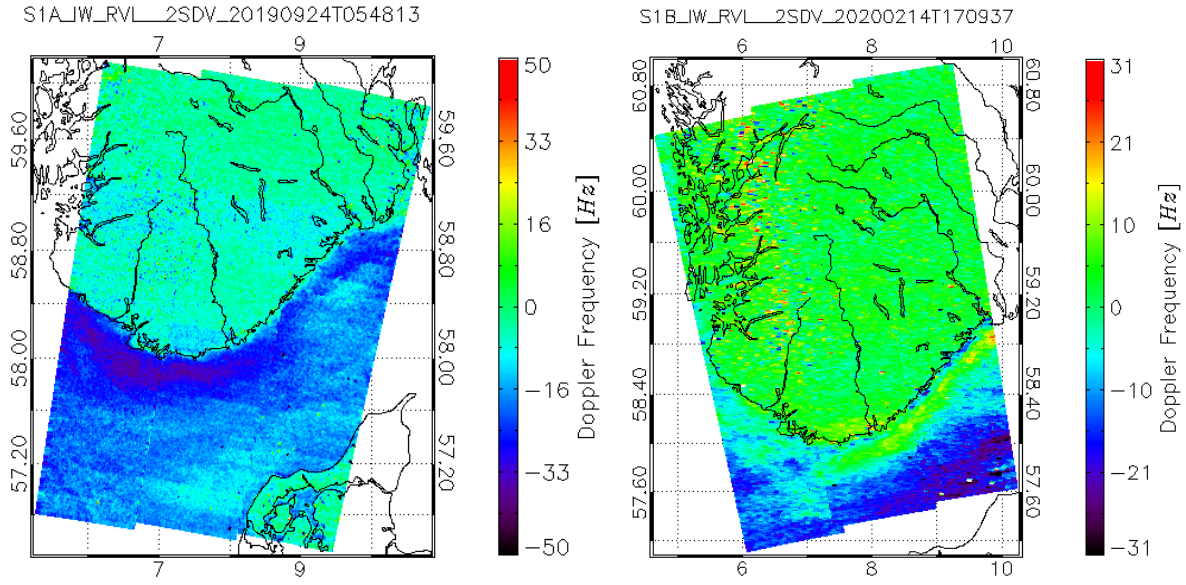


a) b)

Figure 8: a) Calibrated S1a DC image acquired in descending mode over Southern Coast of Norway. b) Calibrated S1b DC images acquired in ascending mode over the same area. In both images we see a clear signature of the Norwegian coastal current.

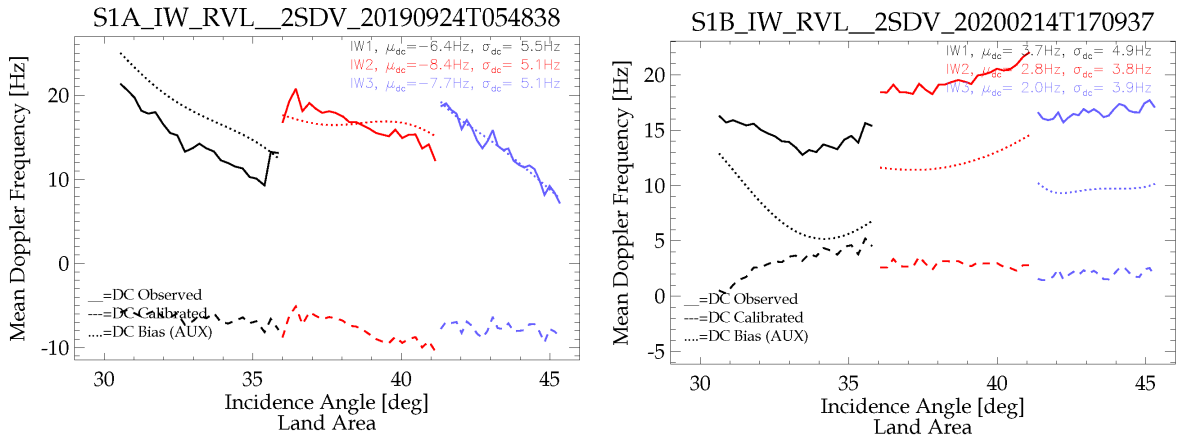


a) b)

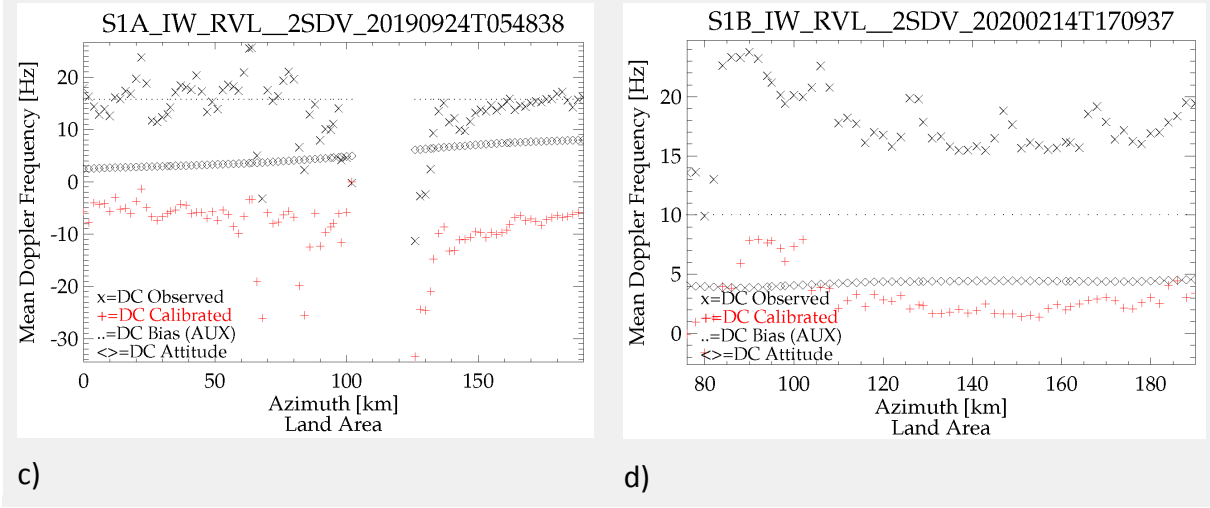


c) d)

Figure 9: (a,b) Mean S1 DC across track. (c,d) Mean S1 DC along track. Left plots are from S1A and right plots are from S1B. The data corresponds to the same products as shown in Figure 9. All data acquired over land areas.

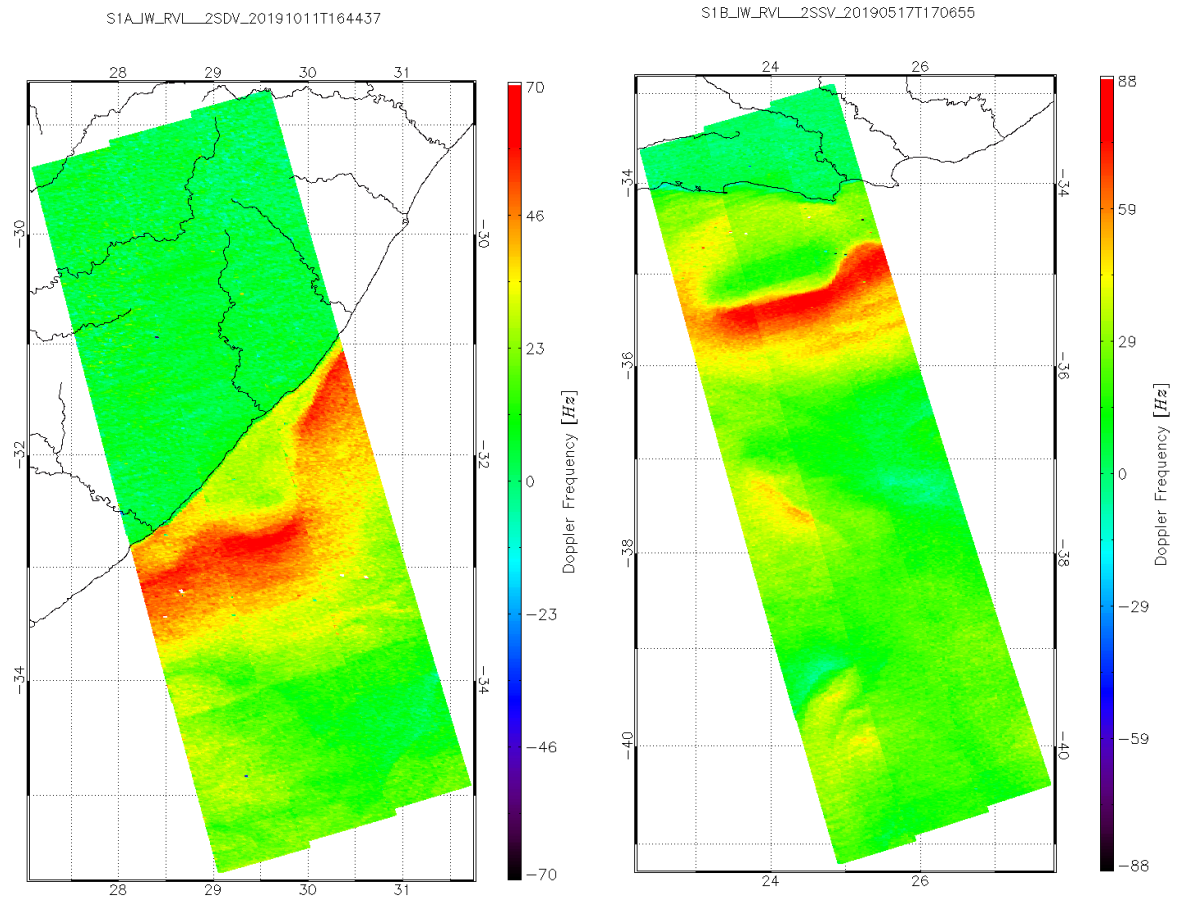


a) b)

Figure 10: a) Calibrated S1a DC image acquired in ascending mode over Agulhas. b) Calibrated S1b DC images acquired in ascending mode over the same area. In both images we see a clear signature of the Agulhas current

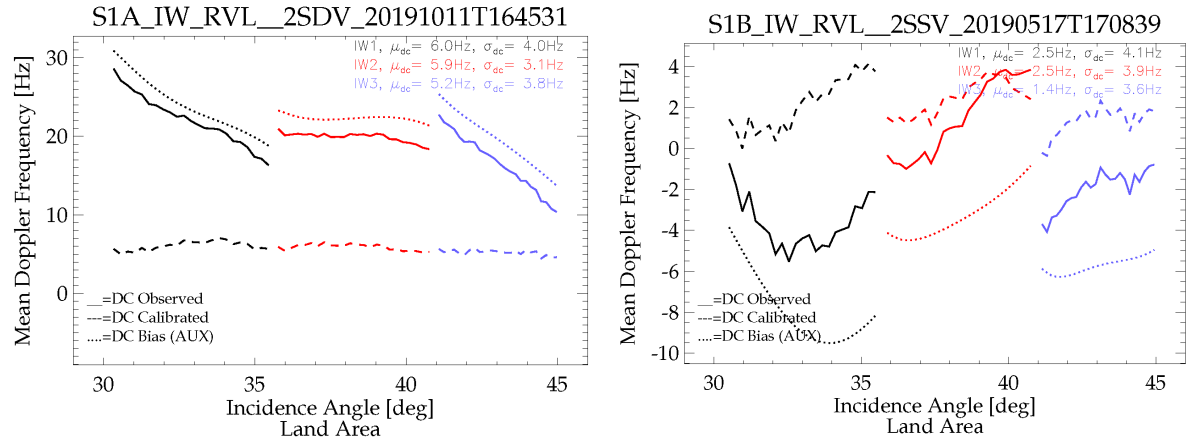


a) b)

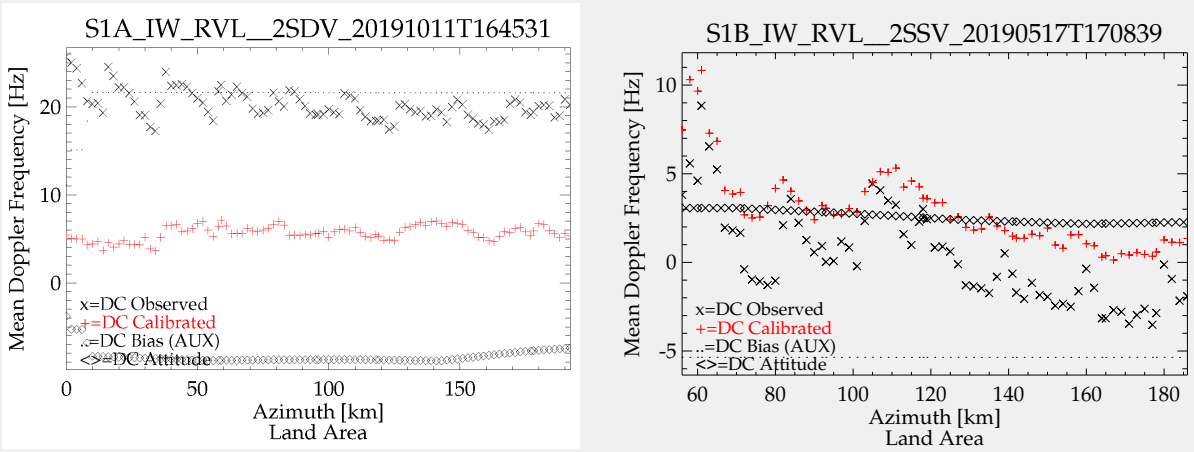


c) d)

Figure 11: Mean DC across track. Data acquired over Agulhas. Left plot is from S1A and lower is from S1B. Same products as in Figure 9. All data acquired over land areas.

We see from Figure 8 and 11 that both the overall bias and the DC jump between sub-swaths are significantly reduced. However, in the S1b data set we clearly observe larger jumps in DC between sub-swaths than in S1a.

The overall performance of the calibrated S-1 IW OCN RVL products from the Skagerak and Agulhas areas are summarized in Figure 12, Table 4 and in Figure 13, Table 5, respectively. The data set comprises 39 S1a IW and 55 S1b IW products from Skagerak and similar number of products acquired over Agulhas.

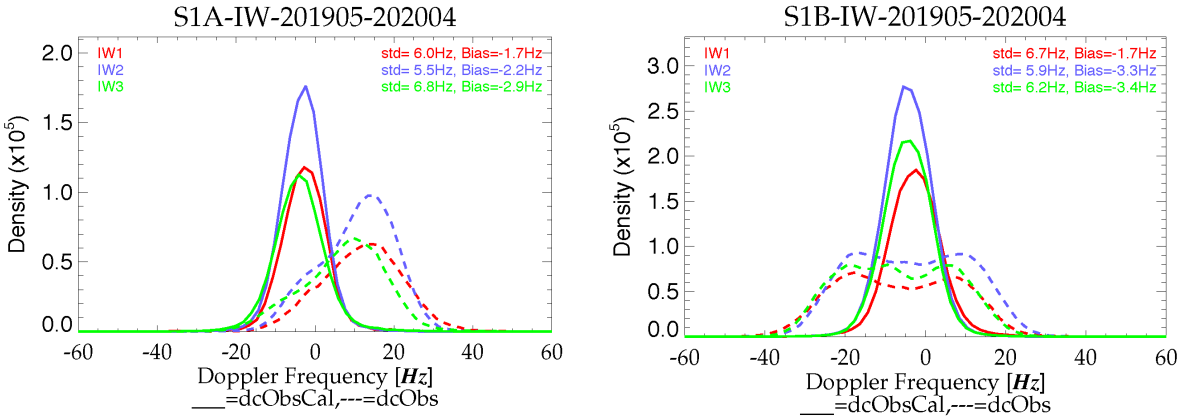


a) b)

Figure 12: Histogram of S1a (left) and S1b (right) IW DC before and after calibration. Data from Skagerak. All data acquired over land areas.

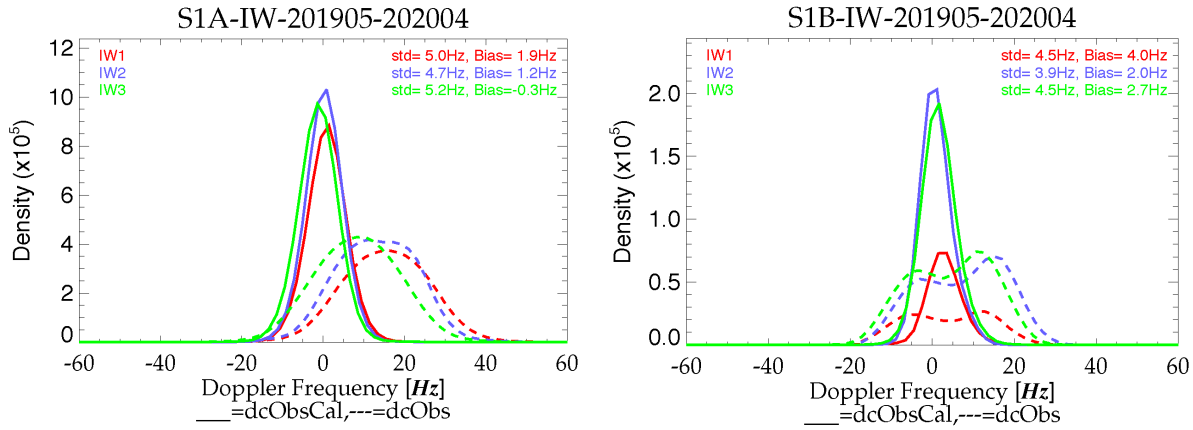


a) b)

Figure 13: Histogram of S1a (left) and S1b (right) IW DC before and after calibration. Data from Agulhas. All data acquired over land areas.

We observe that the reduction in the standard deviation is less compared to the data set over Africa. This is likely due to different characteristics (topography) of the land area, making most of the STD in Norwegian data set to come from DC estimation. The data set over the Norwegian area is also much shorter along track, making the impact of attitude variations less important. We observe from Table 4 that the largest reduction of standard deviation for S1a occurs in IW1 and IW2, and for S1b it is in IW1. This is because it is in these sub-swaths the DC bias shows strongest dependency on incidence angle.

Table 4: Overall performance of S-1 IW calibrated OCN RVL product over Skagerak. All data acquired over land areas.

| S1a IW | | | | | | | | | | | |
|---|---|---|---|---|---|---|---|---|---|---|---|
| IW1 | | | | IW2 | | | | IW3 | | | |
| STD [Hz] | | Bias [Hz] | | STD [Hz] | | Bias [Hz] | | STD [Hz] | | Bias [Hz] | |
| Before | After | Before | After | Before | After | Before | After | Before | After | Before | After |
| 10.3 | 6.0 | 12.7 | -1.7 | 9.6 | 5.5 | 11.5 | -2.0 | 10.6 | 6.7 | 8.1 | -2.9 |

| S1b IW | | | | | | | | | | | |
|---|---|---|---|---|---|---|---|---|---|---|---|
| IW1 | | | | IW2 | | | | IW3 | | | |
| STD [Hz] | | Bias [Hz] | | STD [Hz] | | Bias [Hz] | | STD [Hz] | | Bias [Hz] | |
| Before | After | Before | After | Before | After | Before | After | Before | After | Before | After |
| 14.7 | 6.6 | -5.7 | -1.6 | 14.3 | 5.9 | -2.7 | -3.3 | 13.6 | 6.1 | -5.8 | -3.3 |

Table 5: Overall performance of S-1 IW calibrated OCN RVL product over Agulhas. All data acquired over land areas.

| S1a IW | | | | | | | | | | | |
|---|---|---|---|---|---|---|---|---|---|---|---|
| IW1 | | | | IW2 | | | | IW3 | | | |
| STD [Hz] | | Bias [Hz] | | STD [Hz] | | Bias [Hz] | | STD [Hz] | | Bias [Hz] | |
| Before | After | Before | After | Before | After | Before | After | Before | After | Before | After |
| 10.4 | 4.9 | 16.5 | 1.9 | 9.9 | 4.7 | 14.1 | 1.2 | 10.4 | 5.2 | 9.3 | -0.3 |

| S1b IW | | | | | | | | | | | |
|---|---|---|---|---|---|---|---|---|---|---|---|
| IW1 | | | | IW2 | | | | IW3 | | | |
| STD [Hz] | | Bias [Hz] | | STD [Hz] | | Bias [Hz] | | STD [Hz] | | Bias [Hz] | |
| Before | After | Before | After | Before | After | Before | After | Before | After | Before | After |
| 10.5 | 4.5 | 4.7 | 3.9 | 10.5 | 4.5 | 8.4 | 1.9 | 10.1 | 4.4 | 5.5 | 2.6 |

# 4. Summary

The accuracy and precision of the calibrated DC frequency of S1 WV and IW acquisitions are assessed using data acquired over both land and ocean areas. The attitude DC and the observed DC show mostly similar trends along track over land areas. We conclude that the estimated attitude data works well in reconstructing the attitude DC signal. The calibrated DC are relatively constant over each sub-swath but with small sub-swath dependent offsets, in particular for S1b IW mode. This shows that the AUX DC bias works well in predicting the relative variation of DC over sub-swaths for, but for S1b IW a few Hz offset between sub-swaths are still observed. This indicates that there is a change in antenna characteristics that is on a timescale not capture with the procedure used to generate the mean DC bias stored in the AUX DC file. It may also partly be caused by the observed difference (bias) between the Level 2 DC and the raw data DC used to generate the AUX_DCBIAS file.

The DC calibration reduces the standard deviation (STD) and bias (BIAS) significantly for both satellites and for all swaths. Assessment of the performance of global WV data shows a STD around 6Hz, while the BIAS is less than 2 Hz. The performance is very similar for both satellites and for both swaths. For IW the STD is similar, but the bias is slightly higher and different between sub-swaths for S1b. These variations are mainly due to the change in antenna characteristics on a timescale not captured with the procedure used to generate the mean DC bias stored in the AUX_DCBIAS file. Such changes may come from the temperature compensations applied to the antenna. This mainly affects the IW mode where it is also clearly visible in some scenes. For WV mode it mainly impacts the overall performance statistics. We conclude that S1 WV mode has achieved a performance (i.e. accuracy and precision) within the requirement for climatology mapping of global ocean current features. For IW mode, we have achieved a precision within the requirement, but use of land areas within the scene is still required to achieve the required accuracy for a single scene. However, better prediction of when the temperature compensation is activated and its impact on the antenna characteristics can further help improve the performance of the Level 2 OCN DC. Alignment of the Level 2 DC and raw data DC estimation (on average there should be no bias) will also help reduce the DC offset observed between sub-swaths of IW mode.

## References

OceanDataLab. (2019). S-1 RVL DIL4: Algorithm Description Document. Esrin/ESA.

Moiseev, A., Johnsen, H., Johannessen, J. A., Collard, F., & Guitton, G. (2020). On removal of sea state contribution to Sentinel-1 Doppler shift for retrieving Reliable Ocean surface current. Journal of Geophysical Research: Oceans, 125, e2020JC016288. https://doi.org/ 10.1029/2020JC016288

Bourassa et. al., (2019). "Remotely Sensed Winds and Wind Stresses for Marine Forecasting and Ocean Modeling", Front. Mar. Sci., 23 August 2019, https://doi.org/10.3389/fmars.2019.00443

Ardhuin F., M. Louis, Rascle N., Forget P., Roland A., (2009). "Obsevation and Estimation of Lagrangian, Stokes, and Eulerian Currents Induced by Wind and Waves at the Sea Surface", J. of Physical Oceanography, Vol.39, pp.2820-2838, DOI:10.1175/2009JPO4169.1

Röhrs J., Sperrevik A.K., Christensen K.H., Broström G., Breivik Ø., (2015). "Comparison of HF radar measurements with Eulerian and Lagrangian surface currents", Ocean Dynamics (2015) 65:679–690, DOI: 10.1007/s10236-015-0828-8

Romeiser R., Suchandt S., Runge H., Steinbrecher U., and Grünler S., "First analysis of TerraSAR-X along-track InSAR-derived current fields," IEEE Trans. Geosci. Remote Sens., vol. 48, 2010, pp. 820–829.

Romeiser R., Runge H., Suchandt S., Kahle R., Rossi C., and Bell P.S., "Quality assessment of surface current fields from TerraSAR-X and TanDEM-X along-track interferometry and Doppler centroid analysis," IEEE Trans. Geosci. Remote Sens., vol. 52, 2014, pp. 2759–2772.

Chapron B., Collard F., and Ardhuin F., "Direct measurements of ocean surface velocity from space: interpretation and validation," Journal of Geophysical Research, vol. 110, no. C07008, (2005), doi:10.1029/2004JC002809.

Collard, F., Mouche, A., Chapron, B., Danilo, C., & Johannessen, J. (2008). Routine High Resolution Observation Of Selected Major Surface Currents From Space. *Proceedings of SEASAR 2008.* Frascati.

Mouche, A. A., Collard, F., Chapron, B., Dagestad, K. F., Guitton, G., Johannessen, J. A., Hansen, M. W. (2012). On the use of doppler shift for sea surface wind retrieval from SAR. *IEEE Transactions on Geoscience and Remote Sensing, 50*(7 PART 2), 2901-2909. 10.1109/TGRS.2011.2174998

Johannessen, J. A., Chapron, B., Collard, F. Kudryavtsev, V., Mouche, A., Akimov, D., & Dagestad, K. F. (2008). Direct ocean surface velocity measurements from space: Improved quantitative interpretation of Envisat ASAR observations. *Geophysical Research Letters, 35*(22), 1-6. https://doi.org/10.1029/2008GL035709

Hansen, M. W., Collard, F., Dagestad, K.-F., Johannessen, J., Fabry, P., & Chapron, B. (2011). Retrieval of sea surface range velocities from envisat ASAR doppler centroid measurements. *IEEE Transactions on Geoscience and Remote Sensing, 49*(10 PART 1), 3582-3592. 10.1109/TGRS.2011.2153864

Moiseev, A., Johnsen, H., Hansen, M. W., & Johannessen, J. A. (2020). Evaluation of Radial Ocean Surface Currents Derived from Sentinel-1 IW Doppler Shift Using Coastal Radar and Lagrangian Surface Drifter Observations. *Journal of Geophysical Research: Ocean*. (in review).

Chapron, B., Collard, F., & Ardhuin, F. (2005, 07). Direct measurements of ocean surface velocity from space: Interpretation and validation. *Journal of Geophysical Research: Oceans, 110*, C07008. https://doi.org/10.1029/2004JC002809

Martin, A., Gommenginger, C., Marquez, J., Doody, S., Navarro-Sanchez, V., & Buck, C. (2016). Wind-Wave induced velocity in ATI SAR Ocean Surface Currents: First experimental evidence from an airborne campaign. *Journal of Geophysical Research: Oceans*. https://doi.org/10.1002/2015JC011459

Yurovsky, Y., Kudryavtsev, V., Grodsky, S., & Chapron, B. (2019, 4). Sea Surface Ka-Band Doppler Measurements: Analysis and Model Development. *Remote Sensing, 11*, 839. https://doi.org/10.3390/rs11070839

Johnsen, H., Nilsen, V., Engen, G., Mouche, A., & Collard, F. (2016). Ocean doppler anomaly and ocean surface current from Sentinel-1 TOPS mode. *2016 International Geoscience and Remote Sensing Symposium (IGARSS)*, Beijing, pp. 3993-3996. 10.1109/IGARSS.2016.7730038

CLS. (2019). *S-1A & S-1B Annual Performance Report for 2018.* ESA.

Collecte Localisation Satellites. (2019). *Sentinel-1 Product Specification.* S1-RS-MDA-52-7441. ESA.

Tolman, H. L. (2009). *User manual and system documentation of WAVEWATCH III TM version 3.14.* Technical note, MMAB Contribution.

Kudryavtsev, V., Yurovskaya, M., Chapron, B., Collard, F., & Donlon, C. (2017). Sun glitter imagery of surface waves. Part 2: Waves transformation on ocean currents. *Journal of Geophysical Research: Oceans, 122*(2), 1384-1399. https://doi.org/10.1002/2016JC012426

Ardhuin, F., Gille, S. T., Menemenlis, D., Rocha, C. B., Rascle, N., Chapron, B., . . . Molemaker, J. (2017). Small-scale open ocean currents have large effects on wind wave heights. *Journal of Geophysical Research: Oceans, 122*(6). https://doi.org/10.1002/2016JC012413

Alpers, W., & Hennings, I. (1984, 01). A theory of the imaging mechanism of underwater bottom topography by real and synthetic aperture radar. *Journal of Geophysical Research, 891*, 10529-10546. https://doi.org/10.1029/JC089iC06p10529

Mouche, A., & Chapron, B. (2015, 10). Global C-Band Envisat, RADARSAT-2 and Sentinel-1 SAR measurements in copolarization and cross-polarization. *Journal of Geophysical Research: Oceans, 120*. https://doi.org/10.1002/2015JC011149

Chapron, B., Collard, F., & Kerbaol, V. (2004). Satellite synthetic aperture radar sea surface Doppler measurements. *2nd Workshop on Coastal and MarineApplications of Synthetic Aperture Radar*. Svalbard, pp.133-141

Martn, A., Ashish, A., Paul, B., Eugene, B., Zhifeng, C., Craig, C., . . . Andrew, H. (2015). TensorFlow: Large-Scale Machine Learning on Heterogeneous Systems. https://www.tensorflow.or

Laurindo, L. C., Marian, A. J., & Lumpkin, R. (2017). An improved near-surface velocity climatology for the global ocean from drifter observations. *Deep Sea Research Part I: Oceanographic Research Papers, 124*, 73 - 92. https://doi.org/10.1016/j.dsr.2017.04.009

Mouche, A., Chapron, B., Reul, N., & Collard, F. (2008). Predicted Doppler shifts induced by ocean surface wave displacements using asymptotic electromagnetic wave scattering theories. *Waves in Random and Complex Media, 12*(1), 185-196. 10.1080/17455030701564644

Engen G., Johnsen H., “Sentinel-1 Doppler and Ocean Radial Velocity Algorithm Definition”, Norut Report No. 19/2015, S1-TN-NRT-53-0658, version 1.4, ISBN: 978-82-7492-311-9

Johnsen H., Nilsen V., Engen G., Mouche A., Collard F., “Ocean Doppler Anomaly and Ocean Surface Current from Sentinel-1 TOPS Mode”, Geoscience and Remote Sensing Symposium (IGARSS), 2016 IEEE International. 10-15 July 2016 Pages 3993-3996 http://dx.doi.org/10.1109/IGARSS.2016.7730038

Sentinel-1 Product Specification, S1-RS-MDA-52-7441, DI-MPC-PB, Ref: MPC-0240, Issue 3/7, 27/02/2020

Christensen K. H., Sperrevik A. K., Broström G., ” On the variability in the onset of the Norwegian Coastal Current”, American Meteorological Society, DOI: 10.1175/JPO-D-17-0117.1